Available online at www.sciencedirect.com

SCIENCE DIRECT®

Surface Science 579 (2005) 47–57

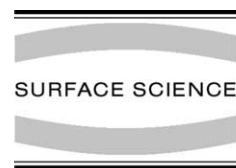

www.elsevier.com/locate/susc

Molecular dynamics simulations of the nano-scale room-temperature oxidation of aluminum single crystals

A. Hasnaoui [a,*], O. Politano [a,*], J.M. Salazar [a], G. Aral [b], R.K. Kalia [b], A. Nakano [b], P. Vashishta [b]

[a] *Universite de Bourgogne, UMR-5613 CNRS, Faculte des sciences Mirande, 9 Av. Alain Savary 21078, Dijon Cedex, France*
[b] *Collaboratory for Advanced Computing and Simulations, Departments of Material Science and Engineering, Physics and Astronomy and Computer Science, University of Southern California, Los Angeles, CA 90089-0242, USA*

Received 19 November 2004; accepted for publication 25 January 2005

Abstract

The oxidation of aluminum single crystals is studied using molecular dynamics (MD) simulations with dynamic charge transfer between atoms. The simulations are performed on three aluminum low-index surfaces ((1 0 0), (1 1 0) and (1 1 1)) at room temperature. The results show that the oxide film growth kinetics is independent of the crystallographic orientation under the present conditions. Beyond a transition regime (100 ps) the growth kinetics follow a direct logarithmic law and present a limiting thickness of ~3 nm. The obtained amorphous structure of the oxide film has initially Al excess (compared to the composition of Al_2O_3) and evolves, during the oxidation process, to an Al percentage of 45%. We observe also the presence of an important mobile porosity in the oxide. Analysis of atomistic processes allowed us to conclude that the growth proceeds by oxygen atom migration and, to a lesser extent, by aluminum atoms migration. In both cases a layer-by-layer growth mode is observed. The results are in good agreement with both experiments and earlier MD simulations.
© 2005 Elsevier B.V. All rights reserved.

Keywords: Molecular dynamics; Oxidation; Aluminum; Thin films

1. Introduction

Thin aluminum-oxide films have technological applications in microelectronics and catalysis, and for protection against wear and corrosion. For example, thin aluminum-oxide films are used in various types of microelectronic devices as a dielectric, diffusion and/or tunneling barrier [1–5],

* Corresponding authors. Tel.: +33 380 39 61 78; fax: +33 380 39 61 32 (A. Hasnaoui), Tel.: +33 380 39 61 72; fax: +33 380 39 61 32 (O. Politano).

E-mail addresses: abdellatif.hasnaoui@u-bourgogne.fr (A. Hasnaoui), olivier.politano@u-bourgogne.fr (O. Politano).

0039-6028/$ - see front matter © 2005 Elsevier B.V. All rights reserved.
doi:10.1016/j.susc.2005.01.043

because of their specific physical and chemical properties (i.e. large dielectric constant (~10), large barrier height for electron tunneling (~2 eV), high corrosion resistance, good thermal and mechanical stability, good adhesion). In particular, oxide passive films that form on aluminum and aluminum alloys in air protect the surface against further oxidation and corrosion [6–8]. For these applications, the thickness, morphology, chemical composition, and the microstructure of the oxide film are of great importance [1,3]. Therefore, it is crucial to understand the involved physico-chemical processes to control and stabilize these films.

Understanding of the processes involved in the oxidation of aluminum is a long-standing research, attracting large amounts of experimental and theoretical work. For instance, several works have been devoted to study the kinetic of the growth mechanism of aluminum-oxides [9–11], the reaction of O_2 molecules with aluminum surfaces [12,13] and the initial transient low mobility of oxygen atoms [14]. The composition, the structure and the morphology of aluminum oxide films has also been studied by other researchers [15–17]. Jeurgens et al. [16] have reported that for low temperatures (<573 K) an amorphous oxide film structure of limiting thickness develops whereas at high temperatures (>573 K) an initially amorphous oxide film forms and gradually transforms into crystalline γ-Al_2O_3. In general, at high temperatures, a parabolic growth rate is followed whereas at low temperatures a logarithmic growth mode is rather found [18]. However, despite these efforts, the atomistic details concerning the structure and the mechanisms governing the onset, growth and termination of aluminum oxidation are largely unknown.

From a theoretical perspective several authors, using a density-functional-theory (DFT), have studied the dissociation process of O_2 on aluminum surfaces [19], the stability of oxygen adsorption sites [20] and the interaction of O_2 with aluminum surfaces [21–24]. However, these techniques are limited to very small clusters of atoms, they are confined to the very initial stage of interaction of oxygen atoms with the metal surface and can not provide information of oxide growth.

Large-scale molecular dynamics (MD) simulations are well suited to overcome these limitations. Since the work of Streitz and Mintmire [25], who developed an interaction potential able to describe the Al/O system taking into account a dynamic charge transfer among atoms, MD simulations of the oxidation of more realistic samples became possible. Ogata and Campbell [26] and Campbell et al. [27] have performed the first successful (as far as we know) MD simulations of aluminum oxidation process on spherical nanoclusters, and they found that the oxide film presents a limiting thickness of 3–4 nm. They also found that the oxide film has an amorphous structure consisting of mixed octahedral and tetrahedral configurations. However, these studies (with spherical nanoclusters) did not allow to study the effect of the crystallographic orientation of the substrate, and did not provide a detailed atomistic description of the oxide film structure.

In the present work, we investigate the oxidation of Al-single crystals at 300 K, with three different surfaces ((100), (110) and (111)) using MD simulations based on the interaction potential of Streitz and Mintmire [25]. In the next section, we will describe the used computational method. In the results section, we will show the effect of the crystallographic orientation on the growth kinetics. We will also show how the structure of the oxide film changes during the advance of the oxide thickness. The pair distribution function, the angular distribution and the coordination inside the oxide film are compared to earlier simulations of Campbell et al. [27] and to the experimental work of Lamparter and Kniep [17]. Detailed atomistic analysis will allow us to describe in more details the amorphous structure of the oxide and to gain a physical insight in the growth mechanism via the observation of the atomistic displacements during the oxidation.

2. Computational method

We have developed a new MD simulation code that is based on a highly reliable interaction scheme developed by Streitz and Mintmire [25]. In this potential, the total energy of the crystal is

divided into an electrostatic energy (Es) that is ion charge dependent and a non-electrostatic energy that is ion charge independent (embedded atom method (EAM) potential). A Finnis–Sinclair [28] form is chosen for the EAM potential. This interaction potential (Es + EAM) has been shown to be efficient in describing the cohesive energy, structure, and elastic properties of both fcc aluminum and α-alumina [25].

The Coulomb interaction can be accurately computed by the Ewald summation technique [29], which can be applied in the case of three-dimensional (3D) periodic boundary conditions (PBC). However, the summation of the Coulomb interaction is the main problem in surface applications. Several approximations to this issue have been proposed [30,31] but these methods failed to treat a relatively thick slab as that used in the present work. In this work, for generating the surfaces, the x-direction is artificially increased by adding two vacuum slabs on each side of the fcc aluminum substrate [32]. The unit cell (see Fig. 1) was then repeated infinitely throughout the 3D-space by applying the periodic boundary conditions. This technique allows to create a 2D-slab geometry where the conventional 3D-Ewald summation can be applied. Yeh and Berkowitz [33] showed that the inclusion of a correction term for the slab geometry gives satisfactory results and does not introduce any significant computational difficulties. As shown in Fig. 1, the positions of aluminum atoms in the substrate range, in the x-direction, from $-L_x/2$ to $+L_x/2$ whereas the vacuum is between $-L_x$ and $-L_x/2$ on one side and between

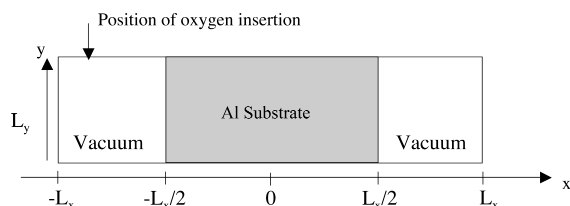

Fig. 1. A schematic picture describing the unit cell of the Al-substrate and the two vacuum slabs surrounding it. The box x/y axes are shown together with the relative sizes. The box size along the z-direction (L_z) is equal to that along the y-direction (L_y). The O_2 molecules are inserted at $1.5\,r_c$ from the oxide layer (r_c is the cutoff radius of the interaction potential).

$+L_x/2$ and $+L_x$ on the other side (with $L_x = 40$ Å). Note that we have also increased the simulation box size along the x-direction to $3L_x$ (i.e. a vacuum slab of $2L_x$) and we observed that it does not improve the accuracy. Given that the CPU time is closely related to the number of k-space vectors, which rapidly increases with the total box size, we prefer keeping the size $2L_x$ and gain in computation time. The simulations were performed with a cutoff radius (r_c) of 6 Å for the interaction potential and $(40 \times 10 \times 10)$ k-vectors for a box size of $(80 \times 20 \times 20)$ Å^3.

The samples created in this manner are then subjected to an equilibration procedure, which starts by increasing the temperature, in steps of 20 K from 0 K to 300 K. For each temperature a run of 1000 MD steps using isokinetic MD was performed. These first equilibration runs are performed by ignoring the dynamic charge transfer between aluminum atoms since the charges are assumed to be zero for a pure metallic system. An extra equilibration run of 1000 steps at 300 K was performed including the charge dynamics and, as expected, showed that the atomic charges fluctuate around a zero value in the pure metal with a magnitude of $\pm 0.06e$ (where $e = 1.6 \times 10^{-19}$ C) at the two outer layers and of $\pm 0.02e$ in the bulk.

After the equilibration runs, we start to oxidize the aluminum by introducing O_2 molecules in the vacuum slab at an x-distance of $1.5\,r_c$ from the aluminum surface. Their y- and z-positions are randomly chosen. O_2 molecules are introduced at 300 K with their velocities randomly chosen from a Maxwell–Boltzmann distribution. A new O_2 molecule is introduced in the gas when the previous O_2 molecule starts to dissociate and form bonds with the Al atoms. With this procedure the gas pressure is maintained constant at $9.8 \times 10^{+5}$ Pa during the whole simulation.

The equations of motion are integrated using a multiple time steps method, with time steps $\Delta t = 1$ fs for the short-range forces and $\Delta t = 5$ fs for the long-range forces. Atomic charges are updated every 100 MD steps such that the electrostatic energy is minimized using a conjugate gradient method with the constraint of the electro-neutrality principle. A Berendsen thermostat

[34] is used to maintain the whole Al–O system at the required temperature (300 K). Note that due to the mass difference between O_2 and Al atoms, the same rescaling factor for aluminum and oxygen leads to a cooling down of oxygen (lighter) atoms and a heating up of aluminum (heavier) atoms. A separate velocity rescaling is then applied to oxygen and aluminum atoms. Constraints are applied to remove the translational and the angular momentums of the substrate [35].

3. Results and discussion

3.1. Growth kinetics of oxide film

We have simulated the oxidation of aluminum-single crystals. The simulations are performed on three different samples with three different orientations ((1 0 0), (1 1 0) and (1 1 1)) and with similar numbers of atoms (∼1000 atoms). The temperature is maintained at 300 K during the whole oxidation process.

Fig. 2 shows the oxygen total uptake as a function of the simulation time up to the limiting thickness, for the three-substrate surface orientations. For the first 200 ps (thickness $d < 2$ nm), the three kinetic curves are similar which suggests that the mechanism of the oxide growth is independent of the crystallographic orientation. After 200 ps, we observe a slight difference, which can reasonably be assigned to statistical fluctuations. This orientation independent effect is due to the oxide amorphous structure that inhibits any relation of epitaxy between the oxide and the metal during the growth process. The simulations stopped once we observe ejection of an AlO_4 fragment from the sample surface. Campbell et al. [27] have performed an MD simulations experiment in the microcanonical ensemble (without heat dissipation) and they have observed, after 50 ps, that small Al_xO_y fragments are ejected from the nanocluster surface indicating that the nanocluster is melting on the surface region. In this work and despite of the dissipation route via the Berendsen thermostat [34], we observe similar processes (e.g. after 500 ps for the (1 0 0) and (1 1 0) surfaces) when the film thickness tends to the limiting value. Indeed, when approaching the limiting regime, oxygen incorporation into the oxide film is impeded and the accumulation of dissociated oxygen atoms at the oxide surface (oxide/gas interface) leads to a heating of this interface that is difficult to dissipate. In experimental works, at low temperatures, the growth kinetic curves present a saturation regime where the growth rate tends to vanish. However, in our simulation we are only able to reach a regime of low growth rate while the saturation regime should be reached for very long times that are not accessible to MD simulations. We therefore use in this work the expressions "limiting regime" and "limiting thickness" to qualify this regime of low growth rate.

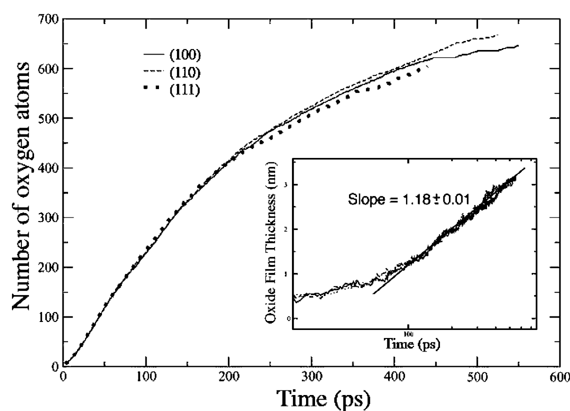

Fig. 2. Oxidation kinetic curves of the (1 0 0), (1 1 0) and (1 1 1) surfaces. These curves represent the total uptake (as a number) of oxygen atoms versus exposure time. The inset shows the oxide film thickness versus time in a semi-logarithmic plot.

After 450 ps, the kinetic curves of the (1 0 0) and (1 1 0) surfaces show a limiting regime where the total uptake is approximately 630 and 660 oxygen atoms, respectively. The simulation of the (1 1 1) surface has been stopped around 450 ps but the tendency of the kinetic curve shows that it should in principle tend to the limiting regime at a similar total uptake value.

The oxide film thickness is defined as the distance between the x-positions of the deepest oxygen atom and the external aluminum atom. This seems to be a rough estimation of the thickness but we have also done a test where we have averaged the x-position over the oxygen atoms laying at the inner interface (2 Å layer) and over

aluminum atoms laying on the outer oxide–gas interface (2 Å layer). The distance separating the two average positions defines the oxide film thickness. The results did not show any difference in the kinetic curves and did not even reduce the fluctuations, which suggests that the straightforward determination is sufficient. The inset in Fig. 2 shows the curves of the oxide film thickness versus the oxidation time (exposure time) for the three aluminum surfaces in a semi-logarithmic representation. In this plot we see that the oxidation of the three surfaces present a limiting thickness, which reached ~3.1 nm, 3 nm and 2.9 nm, at 500 ps, 500 ps and 420 ps, for the (100), (110) and (111) surfaces, respectively. These values corroborate the results obtained in [27] where the oxide thickness reached a limiting value of ~3–4 nm. The three curves obey a direct-logarithmic growth kinetics (a linear behavior in the inset in Fig. 2), although for the early times (>100 ps) the curves deviate from this law due to a transient regime. Note that the inverse logarithmic and parabolic fits fail to describe correctly these kinetic curves for the three faces. Moreover, this growth mode, following a direct logarithmic law, corresponds to a microscopic mechanism where ion movement occurs via extended defects [11], which is the case in the present work.

3.2. Oxide film structure

We have analyzed the structure of the oxide film during the whole oxidation process. First, we have computed the pair distribution function (PDF) of the atoms inside the oxide film including the partial PDFs for each type of pairs of atoms (see Table 1). For the Al–Al pair distribution, we observed a first peak around 2.9 Å (Fig. 3a), which corresponds to the first nearest neighbor distance in the fcc Al lattice. A second peak is detected at around 4 Å, which is the second nearest neighbor distance in the fcc Al lattice, in particular for early times. This last peak disappears during the development of the oxide film whereas the first one subsists even at the limiting regime.

For the O–O pair distribution function, a peak is detected at 3.1 Å for times less than 100 ps and then it shifts progressively to reach 2.8–2.9 Å at the limiting regime (Fig. 3a). Another peak appears progressively during the development of the oxide film around 2.1–2.2 Å. This last peak is close to the O–O peak (at 2.5 Å) of the Al_2O_3 crystalline structure.

The Al–O PDF showed a peak around 1.8 Å during the whole oxidation process, except for the very early stage that corresponds to the oxide nucleation. A typical example of this PDF is plotted in Fig. 3a. The distance of this peak is very close to the typical first Al–O distances of 1.85 Å and 1.97 Å existing in the Al_2O_3 crystalline structure. Moreover, it corresponds to the reported Al–O bond length in amorphous aluminum oxide films that ranges from 1.8 to 1.9 Å [17,27]. Fig. 3a is in good quantitative and qualitative agreement with both the simulation results of Campbell et al. [27] and the experimental results of Lamparter and Kniep [17] (see Table 1). The latter authors have reported 3.2, 2.8 and 1.8 Å for the Al–Al, O–O and Al–O bond length, respectively, whereas in our simulations we have found 2.9, 2.8 (and 2.1 to a less extend) and 1.8 Å, respectively. As shown in Table 1, we obtain a good agreement with numerical and experimental approaches although that we observe a supplementary small peak at 2.1 Å for

Table 1
Values of the first nearest bond length R_{ij} for the different pairs of atoms and the corresponding coordination numbers Z_{ij}, in the case of the (100) surface simulation taken at 384 ps

	This work		Lamparter and Kniep [17]		Campbell et al. [27]	
	R_{ij} (Å)	Z_{ij}	R_{ij} (Å)	Z_{ij}	R_{ij} (Å)	Z_{ij}
Al–Al	2.9	7.5	3.2	6	–	–
O–O	2.8–2.9	9.1	2.8	8.5	–	–
Al–O	1.8	4.1	1.8	4.1	1.8	3.9

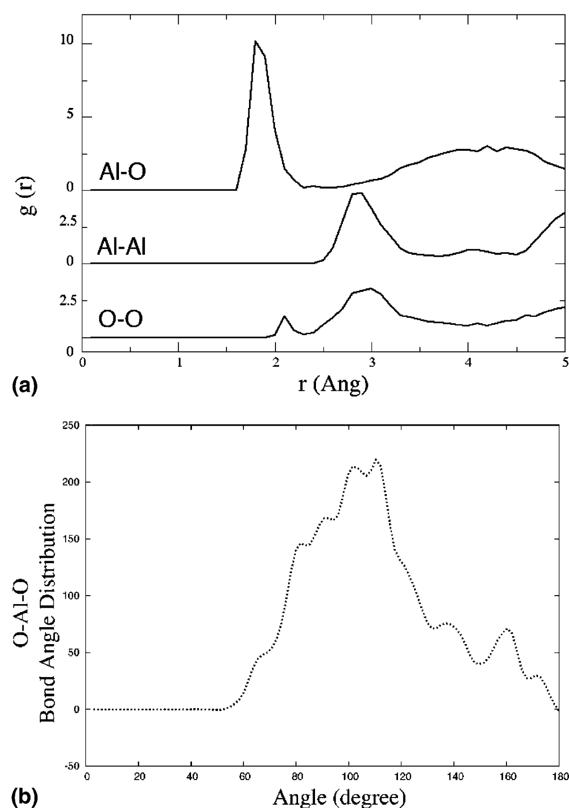

Fig. 3. An example of (a) the pair distribution function of the Al–O bond and (b) the Al–O–Al bond-angle distribution function. These distributions are taken at 384 ps exposure in the case of the (100) surface simulation.

the O–O distance, which attenuates upon annealing at 600 K. This latter peak is not reported in Table 1.

Moreover, we have calculated the average coordination number Z_{ij} of each type of pair (Al–O, Al–Al, and O–O). The result is presented in Table 1 by the values of Z_{ij}'s that were determined from the atomic cluster statistics using a sphere radius $R = 1.2r_o$, where r_o is the value of the first peak of each PDF curve. We obtained average values of 7.5, 9.1 and 4.1 for the coordination numbers of the three bond length, respectively. This is again in agreement with the experimental results in [17] that reported 6, 8.5 and 4.1, respectively (Table 1). The value of 4.1 corresponding to the Al–O bond length is an average value over the whole oxide film and is in good agreement with the simulation results of Campbell et al. [27] who found 3.1, 3.9 and 4.3 at the metal–oxide interface, within the oxide and at the oxide–gas interface respectively.

The consistency of the 1.8 Å value for the Al–O bond length and the evolution of the different partial pair distribution functions suggests that the AlO_4 tetrahedron plays an important role in the building up of the amorphous oxide film structure as suggested by Lamparter and Kniep [17]. However, in contrast to these authors and in agreement with Campbell et al. [27], we think that the AlO_6 octahedron structure plays a non-negligible role in the building up of the final amorphous structure, since the coordination number 6 for the Al–O bond is quite frequent in the obtained structure. In fact the distribution of the Al–O coordination number in the oxide film can be characterized by the frequencies (see Table 2): Z(O–Al) = 3(10%), 4(41%), 5(28%) and 6(15%) for times beyond 200 ps. Note that these values are obtained by averaging over times beyond 200 ps for the (100) surface simulation and are also obtained for the two other orientations. However, during the first 200 ps the coordination Z(Al–O) = 4 was found to be present at 60%, which suggests that initially the amorphous structure of the oxide film is built up by AlO_4. As the oxide develops the AlO_6 contributes more and more to the structure to finally reach a value around 15% (Fig. 4). Looking at the coordination profiles, we have seen that for early times ($t < 1$ ps, $d < 1$ nm), the coordination of Al–O bond is around 4 for the whole oxide film. During the development of the film, it becomes more heterogeneous and gradually changes from 4 (at the metal–oxide interface) to 6 (at the oxide–gas interface).

Fig. 3b shows a typical example of the angular distribution function of the atoms belonging to the oxide film taken at 384 ps. This distribution presents a main peak around 110° as found by Campbell et al. [27]. However, whereas Campbell et al. [27] found another peak between 80° and 90°, we found a second peak around 70° but not as well defined as in their work. Moreover, we see a third peak around 160°. These last two peaks are not stable; they shift towards smaller and larger values but also may disappear during the development of

Table 2
The distribution of the different coordination numbers of the Al–O bond, in the case of the (1 0 0) surface simulation

Z	Percentage of atoms	
	This work	Lamparter and Kniep [17]
3	10	20
4	41	56
5	28	22
6	15	–
Other	6	–

The simulation values are taken as average values over times beyond 200 ps.

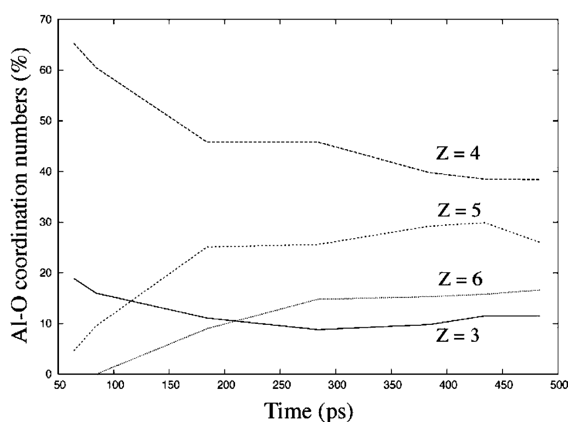

Fig. 4. Time evolution of the different coordination numbers of Al–O bond (Z = 3, 4, 5 and 6) as shown in the figure.

the oxide film whereas the other sub-peaks observed in Fig. 3b are thought to be due to statistical fluctuations. Indeed, these sub-peaks are not reproduced for other times. Nevertheless, the angular distribution function resembles qualitatively to the one obtained by Campbell et al. [27] and the relative disagreement may be due to the sizes of the simulation samples.

We have also analyzed the composition of the oxide film structure during its growth and plotted the results in Fig. 5. We observe that the total atomic density increases rapidly during early times (<50 ps) and then tends to a constant value around 0.09 atom/Å^3. The two partial densities show a rapid increase of both aluminum and oxygen atoms for short times and then the oxygen density becomes almost constant (0.05 atom/Å^3) whereas that of aluminum decreases with time and reaches

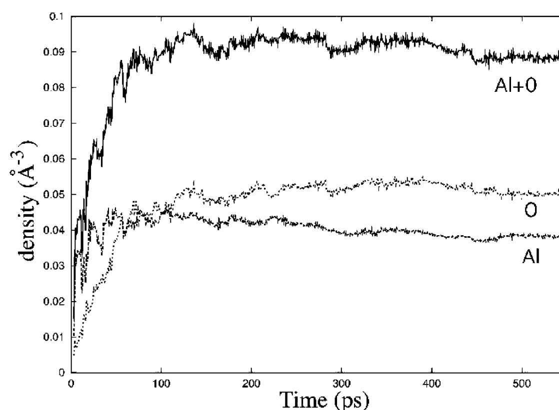

Fig. 5. The plot of oxygen, aluminum and total atomic densities in the oxide film versus exposure time for the (1 0 0) surface.

a value of 0.04 atom/Å^3. This trend confirms our first analysis, which suggests that the population of the AlO_6 structure increases with time. The relative O/Al composition ratio increases rapidly for short times (<100 ps) and tends to fluctuate between 1.3 and 1.4 for longer times up to the limiting regime. In an experimental work, Jeurgens et al. [15] have found that the initial Al concentration in the grown oxide film increases with increasing temperature. At low temperatures (T < 573 K), an amorphous, Al-deficient (as compared to γ-Al_2O_3) oxide film of 'limiting' oxide-film thickness is formed. During the initial, fast oxidation stage at higher temperatures ($T \geqslant 673$ K), an Al-enriched, amorphous oxide film is formed, which gradually attains the stoichiometric composition of Al_2O_3 and becomes crystalline γ-Al_2O_3 during the second slow oxidation stage. In our simulation we found that the percentage of aluminum atoms in the oxide film decreases from 90% and tends asymptotically to 45% (0.04 atom/Å^3) for times larger than 300 ps but never reached the stoichiometric composition of Al_2O_3. The amorphous oxide film is Al-enriched as in the case of high temperatures in the work of Jeurgens et al. [15]. We should also note that the oxide limiting thickness does not extend beyond 1 nm in Jeurgens et al. [15] work, for low temperatures whereas for high temperatures it reaches values larger than 3 nm if we extrapolate their data to long times. We think that this discrepancy between the present results

and Jeurgens work, concerning the structure of the oxide at low temperatures, might be due to the high pressure used in the MD simulation, which is $9.8 \times 10^{+5}$ Pa (Jeurgens et al. 1.33×10^{-4} Pa). Such a high-pressure regime is an accepted caveat of the simulation technique, and is necessary to reduce the time-scale problem inherent to the MD method.

Detailed atomic visualization of the structure showed that the amorphous structure of the oxide contains a non-negligible density of porosity. Fig. 6a shows a snapshot of a 6 Å-thick section of atoms parallel to the oxidized surface (for the (1 0 0) simulation). As we can see from this figure an important number of pores exists in the oxide structure. A temporal analysis revealed that these pores move within the oxide and that their density varies with time. To confirm this, we draw in Fig. 6b another section of atoms from a side view, where we can also see pores, the size of which has been shown to vary from 2 to 8 atomic volumes. We think that the movement and creation/annihilation of these pores is an essential factor for the development of the oxide film since it allows rearrangement of atoms and then incorporation of extra oxygen atoms.

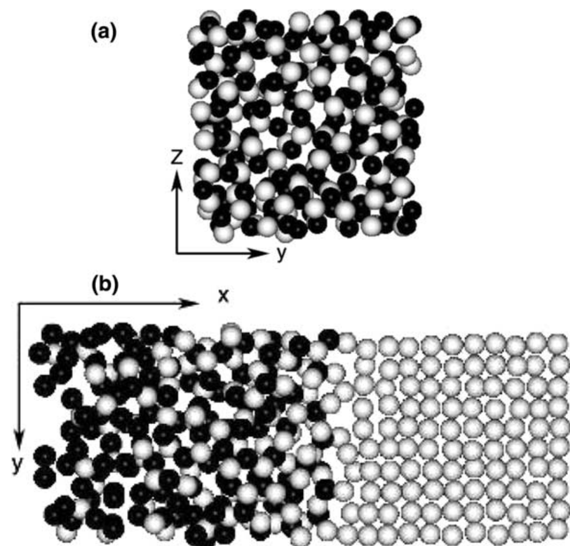

Fig. 6. Snapshots showing examples of the oxide film at 384 ps exposure in the case of the (1 0 0) surface. (a) A top view in the direction vertical to the oxidized surface of a 6 Å-thick section of atoms in the oxide film. (b) A side view of a 5 Å-thick section of atoms showing the oxide and the substrate. Light gray color stands for aluminum atoms and black color for oxygen atoms. Black arrows show the viewing orientation. In this figure we observe the porosity present in the oxide.

Fig. 7 shows the atomic charge distribution plotted as function of the x-distance along the oxidation direction at 384 ps for the (1 0 0) surface. From this figure we see that the substrate bulk presents a charge that fluctuates around zero value. In the oxide film the positive charges are due to aluminum atoms and the negative ones to oxygen atoms. We have checked the zero-charge condition locally in the oxide/aluminum system, and the result of the charge distribution showed fluctuations around zero that reach a maximum of $0.25e$ at the gas/oxide interface and $0.1e$ in the oxide interior. We observe also that this charge is not homogeneous in the oxide and that aluminum atoms are weakly charged close to the metal–oxide interface, greater than $+2e$ in the oxide interior and a small decrease is also observed at the oxide–environment interface. Oxygen atoms are weakly negatively charged at the gas–oxide interface, their charges increase to more negative values to reach a maximum value at a distance of 1 nm from the metal–oxide interface and then decrease to less negative values up to the oxide-metal interface. We notice that there is a strong correlation between the Al coordination (in terms of surrounding oxygen

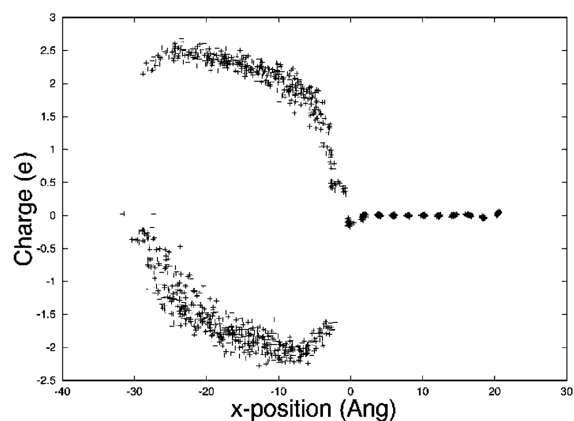

Fig. 7. An example of the charge distribution in the whole Al/O system taken at 384 ps for the (1 0 0) surface. The charge distribution is shown as the charge of each atom in e units (where $e = 1.6 \times 10^{-19}$ C) versus its x-position in the sample.

atoms) and the atomic charge of aluminum. The charge of Al atom increases with their coordination number.

3.3. Atomistic mechanisms

We have performed a new simulation with the same conditions as for our first simulation but this time only one O_2 molecule was inserted during the whole simulation run. In other words, when the O_2 molecule reaches the Al surface, we do not insert a new one to avoid interaction between several pairs of oxygen atoms at the surface. We observed in this case that one oxygen atom remained at the surface layer and formed a tetrahedral configuration with four Al atoms. The second oxygen atom is located close to the first sub-layer of the Al substrate and also formed a tetrahedral configuration. The two oxygen atoms are at a distance of roughly 3.5 Å from each other. No deep penetration was observed (in contrast to the first simulations), which suggests that the oxygen–oxygen interaction and the formation of the oxide unit cell is the process that triggers deeper incorporation at least during the initial stage of oxidation.

We have looked at the atomic displacement between atoms at different times and we have observed that oxygen atoms penetrate towards the metal and try to occupy an interstitial position between the oxide and the metal. Once the first atom reaches a certain depth there is no more forward penetration until this layer is "saturated". In other words, oxygen atoms penetrate to reach the plane n and fluctuate at this plane until its concentration in oxygen atoms reaches a certain critical value, after which oxygen atoms start to move to the plane $n + 1$. Al atoms pass to an interstitial position at the topmost plane in the metal (i.e., at the metal oxide interface) and then they move to the oxide by some interpenetration between the oxide and the metal. This movement, as for oxygen atoms, advances once the metal–oxide interface plane reaches a critical concentration in Al atoms.

This observation is also confirmed by the results in Fig. 8 where we plotted the time evolution of the number of oxygen and aluminum atoms in the oxide layer. We see from this figure that the number of Al atoms evolves by steps. The height of these steps coincides with 50 atoms in the early times, which corresponds to the number of aluminum atoms in a (1 0 0) plane in our samples. For larger times this effect is still observed but less pronounced. Note that this effect is not observed for the number of oxygen atoms in the oxide film (Fig. 8) because this number is defined as a total uptake of oxygen atoms and it should be a smooth function since each time there is only one molecule that penetrates the oxide film (i.e. beyond the topmost aluminum atoms). Nevertheless, we have analyzed the concentration profiles of oxygen and aluminum atoms in the oxide film and we have observed this layer-by-layer mode movement of both types of atoms. Atomistic visualization of the sample has also confirmed this observation. From another side, the concentration profiles of the different species across the oxide are not uniform. The Al concentration increases from the gas/oxide interface to the oxide/metal interface, whereas the oxygen concentration behaves inversely. The assumption of their uniformity in analytical works should be taken carefully in thin oxide films.

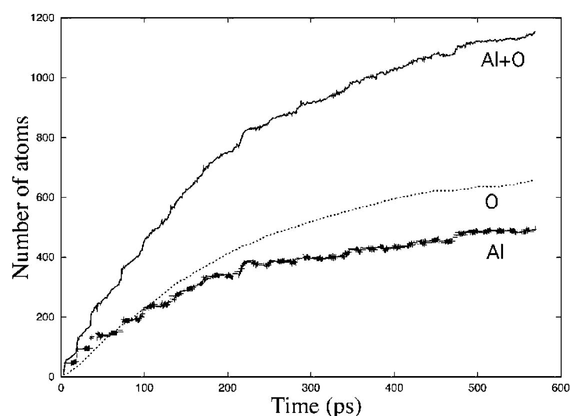

Fig. 8. The plot of oxygen, aluminum and total numbers of atoms in the oxide film versus exposure time for the (1 0 0) surface.

Fig. 9 shows an example of the outward diffusion of aluminum atoms and the inward diffusion of oxygen atoms for the (1 0 0) surface. The atomic displacements are taken between 184 ps and 384 ps exposure times and represented by the black lines

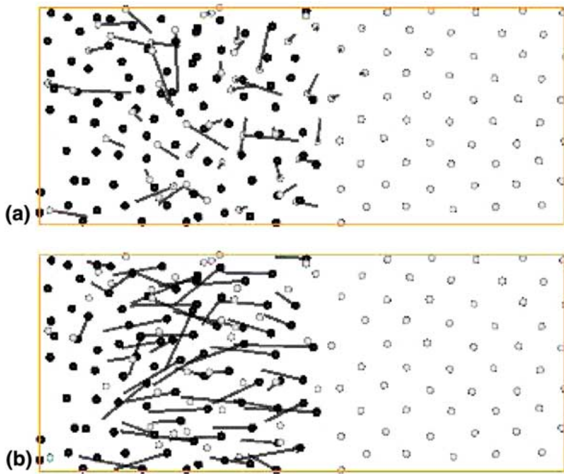

Fig. 9. Snapshot of a section of atoms showing atom positions at 384 ps of exposure for the (1 0 0) surface. The light gray color stands for aluminum atoms and the black color for oxygen atoms. The viewing orientation is the same as in Fig. 6b. The black lines represent the atomic displacements between 184 ps and 384 ps. (a) Displacement vectors of aluminum atoms and (b) displacement vectors of oxygen atoms.

in the figure. Light gray color stands for aluminum atoms and black color for oxygen atoms. Atom positions are shown at 384 ps (i.e. the final positions). Fig. 9a shows the outward migration of Al atoms through the oxide film, and Fig. 9b shows the inward migration of oxygen atoms towards the bulk metal. Note that the shown displacement vectors are viewed in a 2D representation and some of them have a non-zero component in the perpendicular direction. This component represents a migration parallel to the oxidized surface, which has been observed during the oxidation process and more frequently during the earlier stage. Note however, that oxygen migration is more important than aluminum one. The growth of the oxide film is inward and outward because of both inward oxygen migration towards the metal and outward aluminum movement from the metal towards the oxide surface, which is in agreement with the conclusion of Campbel et al. [27].

Note that some of the results presented in this work are taken for the particular case of the (1 0 0) surface but they are also valid for the (1 1 0) and (1 1 1) surfaces, which exhibit similar behaviors.

4. Concluding remarks

We have simulated the oxidation of three aluminum-single crystals with low-index surfaces ((1 0 0), (1 1 0) and (1 1 1)) at 300 K under $9.8 \times 10^{+5}$ Pa. The similarity between the three kinetic curves suggests a growth mechanism that is independent of the crystallographic orientation. This is due to the oxide amorphous structure, which avoids any expitaxial dependence of the growth. A limiting regime is observed at an oxide thickness of ~3 nm. The three curves obey a direct-logarithmic growth kinetic beyond a transient regime. This growth mode corresponds to a microscopic mechanism where ion movement occurs via extended defects (mobile pores in this case) [11]. In this mechanism ion entry into the oxide is considered to become more difficult with increasing oxide thickness because of closing of channels (pores). The analysis of the amorphous oxide structure showed that this structure is in good agreement with experimental and earlier MD simulations results. Initially, the amorphous structure of the oxide film is built up by AlO_4 and as the oxide develops the AlO_6 contributes more and more to the structure reaching a final contribution around 15%. The percentage of aluminum atoms in the oxide film decreases from 90% and tends to 45% for times larger than 300 ps but never reached the stoichiometric composition of Al_2O_3. The results are in good agreement with both experiments and earlier MD simulations. An important density of mobile pores, with their size varying from 2 to 8 atomic volumes, exists in the oxide structure. The movement and creation/annihilation of these pores is an essential factor for the development of the oxide film. Both the inward oxygen migration and the outward aluminum migration proceed by a layer-by-layer mode by initially occupying an interstitial-like position.

Until now, many theoretical studies of metal oxidation have been developed using reaction-diffusion equations [36,37]. This approach concomitant with the use of the dynamical systems theory, allowed to describe qualitatively the time evolution of different oxidation regimes, observed experimentally [38,39]. In these approaches, many parameters are still unknown. We believe that this

work should contribute to develop new models to describe more quantitatively the oxidation process, by incorporating the non-homogeneous composition of the oxide film, its dynamical evolution and the dynamic porosity.

Acknowledgement

We would like to thank the CRI from the University of Burgundy and the CINES from Montpellier for allowing us to access their computer facilities. A. Hasnaoui and O. Politano would like to thank the Conseil Regional de Bourgogne and J.C. Niepce (LRRS—MANAPI group) for their financial support. This work was partially supported in USA by ARL, ARO-MURI, DARPA-PROM, DOE, and NSF.

References

[1] J.M. De Teresa, A. Barthelemy, A. Fert, J.P. Contour, F. Montaigne, P. Seneor, Science 286 (1999) 507.
[2] M. Sharma, S.X. Wang, J.H. Nickel, Phys. Rev. Lett. 82 (1999) 616.
[3] T.W. Hickmott, J. Appl. Phys. 88 (2000) 2805.
[4] E.S. Snow, P.M. Campbell, R.W. Rendell, F.A. Buaot, D. Park, C.R.K. Marrian, R. Magno, Semicond. Sci. Technol. 13 (1998) A75.
[5] A.T.M. van Gogh, S.J. van der Molen, J.W.J. Kerssemakers, N.J. Koeman, R. Griessen, Appl. Phys. Lett. 77 (2000) 815.
[6] F.H. Froes, C. Suryanarayana, D. Eleizer, J. Mater. Sci. 27 (1992) 5113.
[7] A. Tampieri, A. Bellosi, J. Am. Ceram. Soc. 75 (1992) 1688.
[8] E. McCafferty, P.M. Natishan, G.K. Hubler, Interface 2 (1993) 45.
[9] L.P.H. Jeurgens, W.G. Sloof, F.D. Tichelaar, E.J. Mittemeijer, J. Appl. Phys. 92 (2002) 1649.
[10] L.P.H. Jeurgens, W.G. Sloof, F.D. Tichelaar, C.G. Borsboom, E.J. Mittemeijer, Appl. Surf. Sci. 144–145 (1999) 11.
[11] D. Starodub, T. Gustafsson, E. Garfunkel, Surf. Sci. 552 (2004) 199.
[12] O. Benka, M. Steinbatz, Surf. Sci. 525 (2003) 207.
[13] H. Brune, J. Wintterlin, R.J. Behm, G. Ertl, Phys. Rev. Lett. 68 (1992) 624.
[14] M. Schmid, G. Leonardelli, R. Tscheliessnig, A. Biedermann, P. Varga, Surf. Sci. 478 (2001) L355.
[15] L.P.H. Jeurgens, W.G. Sloof, F.D. Tichelaar, E.J. Mittemeijer, Surf. Sci. 506 (2002) 313.
[16] L.P.H. Jeurgens, W.G. Sloof, F.D. Tichelaar, E.J. Mittemeijer, Thin Solid Films 418 (2002) 89;
L.P.H. Jeurgens, W.G. Sloof, F.D. Tichelaar, E.J. Mittemeijer, Phys. Rev. B 62 (2000) 4707.
[17] P. Lamparter, R. Kniep, Physica B 234–236 (1997) 405.
[18] R. Franchy, Surf. Sci. Rep. 38 (2000) 195.
[19] T. Sasaki, T. Ohno, Surf. Sci. 433–435 (1999) 172.
[20] A. Kiejna, B.I. Lundqvist, Surf. Sci. 504 (2002) 1.
[21] Yu.F. Zhukovskii, P.M.W. Jacobs, M. Causa, J. Phys. Chem. Solids 64 (2003) 1317.
[22] Y. Yourdshahyan, B. Razaznejad, B.I. Lindqvist, Solid State Commun. 117 (2001) 531.
[23] Y. Yourdshahyan, B. Razaznejad, B.I. Lindqvist, Phys. Rev. B 65 (2002) 075416-1.
[24] J. Jacobsen, B. Hammer, K.W. Jacobsen, J.K. Norskov, Phys. Rev. B 52 (1995) 14954.
[25] F.H. Streitz, J.W. Mintmire, Phys. Rev. B 50 (1994) 11996.
[26] S. Ogata, T.J. Campbell, J. Phys.: Condens. Matter 10 (1998) 11449.
[27] T.J. Campbell, R.K. Kalia, A. Nakano, P. Vashishta, Phys. Rev. Lett. 82 (1999) 4866.
[28] M.W. Finnis, J.E. Sinclair, Philos. Mag. A 50 (1984) 45.
[29] P.P. Ewald, Ann. Phys. 64 (1921) 253.
[30] J. Hautman, M.L. Klein, Mol. Phys. 75 (1992) 379.
[31] Y.J. Rhee, J.W. Halley, J. Hautman, A. Rahman, Phys. Rev. B 40 (1989) 36.
[32] V.A. Bakaev, Phys. Rev. B 60 (1999) 10723.
[33] I.C. Yeh, M.L. Berkowitz, J. Chem. Phys. 111 (1999) 3155.
[34] H.J.C. Berendsen, J.P.M. Postma, W.F. van Gunsteren, A. DiNola, J.R. Haak, J. Chem. Phys. 81 (1984) 3684.
[35] M.P. Allen, D.J. Tildesley, in: Computer Simulation of Liquids, Clarendon Press, Oxford, 1987.
[36] K.H. Ebert, P. Deuflhard, W. Jäger, in: Modelling of Chemical Reaction SystemsChemical Physics 18, Springer-Verlag, 1980.
[37] G. Bertrand, in: L. Kubin, G. Martin (Eds.), Non Linear Phenomena in Materials Science, 1987, p. 287.
[38] P. Glandsorff, I. Prigogine, in: Thermodynamic Theory of Structure, Stability and Fluctuations, Wiley-Interscience, 1971.
[39] C. Vidal, H. Lemarchand, in: La Réaction Créatrice, Hermann, France, 1988.